

Doping asymmetry in the three-band Hamiltonian for cuprate ladders: failure of the standard model of superconductivity in cuprates

Jeong-Pil Song and Sumit Mazumdar

Department of Physics, The University of Arizona Tucson, AZ 85721

R. Torsten Clay

*Department of Physics & Astronomy, and HPC² Center for Computational Sciences,
Mississippi State University, Mississippi State, MS 39762*

(Dated: today)

The relevance of the single-band two-dimensional Hubbard model to superconductivity in the doped cuprates has recently been questioned, based on Density matrix Renormalization Group (DMRG) computations that found superconductivity over unrealistically broad doping region upon electron-doping, yet complete absence of superconductivity for hole-doping. We report very similar results from DMRG calculations on Cu_2O_3 two-leg ladder within the parent three-band correlated-electron Hamiltonian. The strong asymmetry found in our calculations are in contradiction to the deep and profound symmetry in the experimental phase diagrams of electron- and hole-doped cuprate superconductors, as seen from the occurrence of quantum critical points within the superconducting domes in both cases that are characterized by Fermi surface reconstruction, large jumps in carrier density and strange metal behavior.

The mechanism of unconventional superconductivity (SC) found in the high- T_c cuprates and other strongly-correlated materials remains an outstanding problem in condensed matter physics, more than three decades after its discovery. At the heart of the problem is the choice of the minimal model for the CuO_2 planes that can account for SC. Since the work of Zhang and Rice, who showed that under certain limits the three-band model of the CuO_2 planes could be reduced to a simpler one-band Hubbard model [1], the majority of theoretical work has focused on the single-band Hubbard model, as well as even simpler approximations such as the t - J model. While cluster variants of dynamical mean-field theory find SC in the doped single-band model on a square lattice [2–9], density matrix renormalization group (DMRG) and quantum Monte Carlo (QMC) calculations have detected absence of long-range superconducting order [10–12].

Accurate description of the band structure of the cuprates within a one-band correlated-electron Hamiltonian requires inclusion of second neighbor hopping t' [13–16]. DMRG calculations have therefore been performed on quasi-one-dimensional cylinders for the t - t' - J model, where t'/t negative (positive) corresponds to hole (electron)-doped regimes. No signature of pairing is found in the negative t'/t region [17]. Surprisingly, strong signature of dominant superconducting pair-pair correlations is found in the positive t'/t region, over a very broad range of electron-doping [17]. Enhanced pairing correlations in the electron-doped region have been confirmed from DMRG calculations on related extended t - J models on one-band 6-leg cylinders [18, 19]. These results are exactly opposite to experimental observation in real cuprates, where significantly higher T_c over a much broader doping region is found with hole doping. The authors of reference 17 have subsequently extended their calculations to the parameter region with nonzero

third neighbor hopping t'' [19]. Absence of pairing in the hole-doped region, and strong pairing tendency over very broad region of electron-doping persist within the t - t' - t'' - J model [20]. Quantum Monte Carlo calculations have claimed long-range superconducting correlations for both electron and hole doping at finite U in the U - t - t' Hamiltonian, with *stronger* pairing on the hole doped side [21]. DMRG calculations for the same model contradict these results, however, and only find pairing on the electron-doped side [22]. The origin of the differences in these numerical results and the more serious discrepancy from experimental observations remain not understood.

The single-band model calculations suggest that there are potential problems with reducing the electronic structure of the CuO_2 planes to Cu-site based effective models. Clearly a comparison of hole- versus electron-doped pairing tendencies within the full three-band correlated-electron Hamiltonian for the cuprates will be more useful in this context. We report here the results of high precision DMRG computations on the three-band two-leg cuprate ladder, over a wide range of hole- and electron-doping. The corresponding single-band Hubbard ladder has been widely investigated in the past [23–27]. The undoped (half-filled) single-band two-leg Hubbard ladder has spin-gapped ground state, with spins on the ladder rungs paired into singlets [28]. Doped holes or electrons (equivalent since the single-band Hubbard ladder has particle-hole symmetry) occupy ladder rungs in pairs, which is favored over unpaired charge carriers that would destroy two singlets instead of one. The ground state of the single-band ladder for weak to moderate doping consequently has a spin gap and exhibits singlet superconducting correlations with quasi-long-range order [23–27, 29]. The above result breaks down for the hole-doped three-band ladder, where a recent DMRG study has shown that even though a spin gap persists in the undoped state, superconducting correlations in the hole-

doped decay *faster* than $1/r$, indicating dominance of charge over pairing correlations at long distances [30]. The decay of pair correlations in this case is caused by pair-breaking hole hopping between the O ions, and is strongest when both Coulomb interactions between holes on the same O and O-O hopping are included [30]. The doped holes in hole-doped cuprates primarily reside on oxygen sites; the results for the hole-doped ladder indicate a breakdown of the Zhang-Rice theory [1]. In what follows we compare hole- versus electron-doped three-band two-leg ladder within high precision calculations.

We consider the Cu_2O_3 two-leg ladder Hamiltonian,

$$\begin{aligned}
 H = & \Delta_{\text{dp}} \sum_{i\sigma} p_{i,\sigma}^\dagger p_{i,\sigma} + \sum_{\langle ij \rangle, \lambda, \sigma} t_{\text{dp}}^\perp (d_{i,\lambda,\sigma}^\dagger p_{j,\sigma} + H.c.) \\
 & + \sum_{\langle ij \rangle, \lambda, \sigma} t_{\text{dp}} (d_{i,\lambda,\sigma}^\dagger p_{j,\sigma} + H.c.) + \sum_{\langle ij \rangle, \sigma} t_{\text{pp}} (p_{i,\sigma}^\dagger p_{j,\sigma} + H.c.) \\
 & + U_{\text{d}} \sum_{i,\lambda} d_{i,\lambda,\uparrow}^\dagger d_{i,\lambda,\uparrow} d_{i,\lambda,\downarrow}^\dagger d_{i,\lambda,\downarrow} + U_{\text{p}} \sum_j p_{j,\uparrow}^\dagger p_{j,\uparrow} p_{j,\downarrow}^\dagger p_{j,\downarrow}
 \end{aligned} \quad (1)$$

In Eq. 1 $d_{i,\lambda,\sigma}^\dagger$ creates a hole with spin σ on the i th Cu-site on the λ -th leg ($\lambda=1,2$) of the ladder, $p_{j,\sigma}^\dagger$ creates a hole of spin σ on the j -th O p orbital. The O-ion can be located on a rung or either leg of the ladder. Parameters t_{dp}^\perp and t_{dp} are the nearest neighbor (n.n.) Cu-O rung and leg hopping integrals, respectively, while t_{pp} is the n.n. O-O hopping integral. The phase relations between the orbitals (see Fig. S1 in Supplemental Material) determine the sign convention for the hopping integrals. We have taken all t_{dp}^\perp as negative, while t_{dp} and t_{pp} alternate signs along the length of the ladder. U_{d} (U_{p}) is the Hubbard repulsion between hole pairs on Cu- d (O- p) orbitals, and $\Delta_{\text{dp}} = \epsilon_{\text{p}} - \epsilon_{\text{d}}$ is the site-energy difference between Cu- d and O- p orbitals. We consider ladders with L rungs and open boundary condition, with rungs at both terminal ends. Calculations are for ladders up to $L = 96$ (192 Cu and 286 O sites) and N holes, with the undoped state corresponding to one hole per Cu site ($N = 2L$). For hole (electron) doping we add (remove) particles and define the hole (electron) doping fraction as δ_{h} (δ_{e}) = $N/(2L) - 1$ ($1 - N/(2L)$). In the following we make comparisons of three-band results with those obtained from single-band Hubbard ladders. The single-band Hubbard repulsion, and the rung and leg hopping parameters are written as U , t and t^\perp , respectively. The single-band doping fraction is written as δ .

We set $|t_{\text{dp}}|=1$ ($t_{\text{dp}}^\perp = -1$) and take other Hamiltonian parameters from recent first-principles calculations, $\Delta_{\text{dp}} = 3$, $U_{\text{d}} = 8$, $U_{\text{p}} = \{3, 4\}$, and $t_{\text{pp}} = \{0.5, 0.6\}$ [15, 16]. These parameters are similar to commonly accepted values [31–33]. We employed an S_z -conserving DMRG algorithm using the ITensor library [34] with real-space parallelization [35]. We used a maximal bond dimension of up to 19000, giving a truncation error of less than 1×10^{-7} . All results were extrapolated to the limit of zero truncation error (see [30] for examples of extrap-

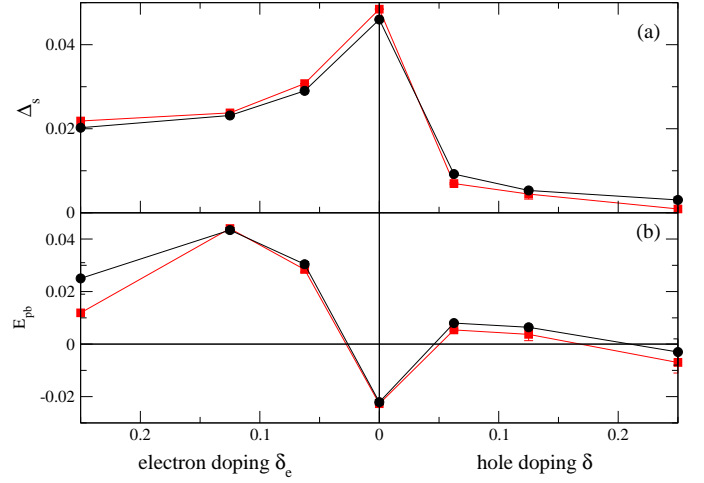


FIG. 1. (Color online) (a) The doping dependence of the extrapolated spin gaps Δ_s in the infinite-length limit ($L \rightarrow \infty$). (b) Pair-binding energy E_{pb} as a function of doping (see text). Circles and squares are for $(U_{\text{p}}, t_{\text{pp}}) = (3, 0.5)$ and $(4, 0.6)$, respectively. A transition to a band state with near-equal populations of charge-carriers on Cu- and O-sites occurs at δ_e larger than that shown here. Lines are guides to the eye.

olation).

The characteristic behavior of the two-leg ladder is determined by its spin gap Δ_s . SC can occur only if the spin gap found in the undoped ladder persists under doping [26, 29, 36]. We calculated Δ_s using finite-size extrapolation from ladders of lengths up to $L=64$. Fig. 1(a) shows the doping dependence of the $L \rightarrow \infty$ extrapolated Δ_s . For the undoped ladder, the behavior of Δ_s against $U_{\text{d}}/|t_{\text{pd}}|$ is very similar to that of the spin gap versus U/t in the single-band Hubbard ladder [23], with a maximum in Δ_s for $U_{\text{d}}/|t_{\text{pd}}| \approx 8$ [30]. However, Δ_s behaves *qualitatively differently* for the electron versus hole doped ladders within Eq. 1. For electron doped ladders Δ_s remains large over a wide doping range, while for hole doping Δ_s decreases rapidly with doping. The normalized spin gap $\tilde{\Delta}_s \equiv \Delta_s(\delta_e)/\Delta_s(\delta_e = 0)$ for the electron doped ladder is comparable to $\tilde{\Delta}_s$ for the single-band Hubbard ladder with $U=8$ and $t^\perp = t$ [37]. For the single-band ladder, $\tilde{\Delta}_s(\delta = 0.125) \approx 0.42$, and is only slightly smaller at $\delta = 0.25$ [37]; in comparison, for the electron doped cuprate ladder with $U_{\text{d}} = 8$, $U_{\text{p}} = 3$, and $t_{\text{pp}} = 0.5$, $\tilde{\Delta}_s(\delta_e = 0.125) = 0.49$ and $\tilde{\Delta}_s(\delta_e = 0.25) = 0.45$. However, for hole doping, $\tilde{\Delta}_s(\delta_h = 0.125) = 0.14$ and $\tilde{\Delta}_s(\delta_h = 0.25) = 0.02$. Δ_s increases with increasing t_{pp} in the undoped three-band model [32]. This effect can be explained in the undoped case from perturbative calculations of the effective exchange J between n.n. Cu spins. About 2/3 of the contribution to J involves t_{pp} , demonstrating the critical role that the oxygen sublattice plays even in undoped cuprates [38]. Our DMRG results show that while Δ_s increases with t_{pp} with electron doping, Δ_s *decreases* with t_{pp} for hole doping. We also calculated the finite-size scaled pair-binding energy

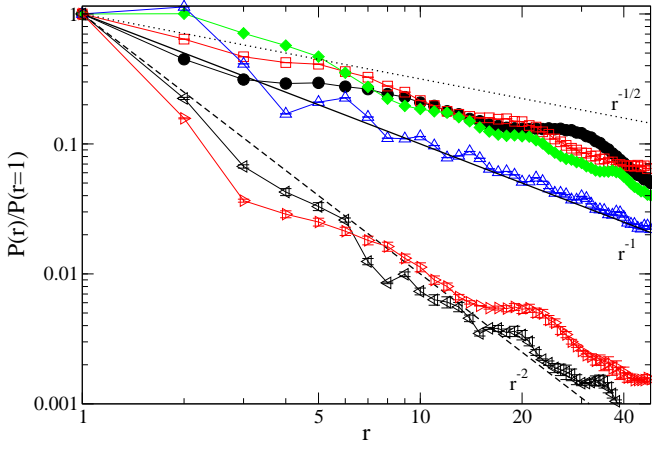


FIG. 2. (Color online) Normalized pair-pair correlation function $P(r)$ as a function of the rung-rung distance r for 96-rung ladders with $U_p = 3$ and $t_{pp} = 0.5$ for several electron dopings δ_e and hole dopings δ_h . Solid, dashed, and dotted lines are power laws r^{-1} , r^{-2} , and $r^{-1/2}$, respectively. Circles, squares, diamonds, and up triangles correspond to electron dopings $\delta_e = 0.0625, 0.0833, 0.125$, and 0.25 , respectively. Right and left triangles are for the hole-doped ladder with $\delta_h = 0.0625$ and 0.125 , respectively[30]. Lines are guides to the eye.

E_{pb} for both hole- and electron-doping, defined as in [39],

$$E_{pb} = 2E(N_{\uparrow} - 1, N_{\downarrow}) - E(N_{\uparrow} - 1, N_{\downarrow} - 1) - E(N_{\uparrow}, N_{\downarrow}). \quad (2)$$

The calculated pair-binding energies, shown in Fig. 1(b), are consistent with the calculated Δ_s .

The doped single band two leg ladder belongs to the Luther-Emery universality class, with gapped spin degrees of freedom and a single gapless charge mode [25, 26, 29, 40]. For the three-band cuprate ladder we define the local charge density operator n_j for the j th unit cell as the sum of the charge density operators for the two Cu sites on a rung, the rung O, and two leg O sites. The charge correlation function is defined as $C(r) = \langle n_i n_j - \langle n_i \rangle \langle n_j \rangle \rangle$, where $r \equiv |i - j|$ is the rung-rung distance. We define the superconducting pair-pair correlation function $P(r) = \frac{1}{2}(\langle \Delta_i^\dagger \Delta_j \rangle + \langle \Delta_i \Delta_j^\dagger \rangle)$, where $\Delta_i^\dagger = \frac{1}{\sqrt{2}}(d_{i,1,\uparrow}^\dagger d_{i,2,\downarrow}^\dagger - d_{i,1,\downarrow}^\dagger d_{i,2,\uparrow}^\dagger)$ creates a spin singlet pair between Cu sites on the i th rung. In the Luther-Emery universality class, charge and pairing correlations decay as power laws in the long distance limit, with asymptotic behavior $C(r) \sim r^{-K_\rho}$ and $P(r) \sim r^{-1/K_\rho}$, respectively. While true long-range superconducting order is absent in a one-dimensional system, for $K_\rho > 1$ pair correlation decay with distance is slower than that of charge correlation and there is quasi-long range superconducting order. Conversely, for $K_\rho < 1$ charge correlations dominate over superconducting quasi-long range order.

The direct approach to determine if superconducting correlations follow a power-law decay with distance involves fitting $P(r)$ against r . To reduce finite-size ef-

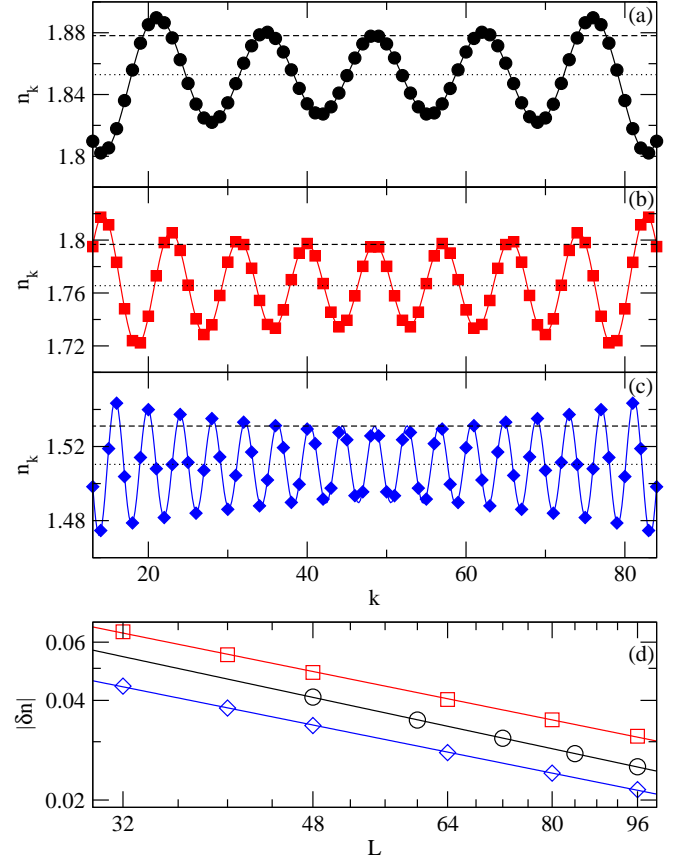


FIG. 3. (Color online) The local charge density profile on a 96-rung ladder with $U_p = 3$ and $t_{pp} = 0.5$ for electron dopings $\delta_e =$ (a) 0.0833, (b) 0.125, and (c) 0.25. The curves are fits to Eq. 3. Dotted and dashed lines represent n_0 and $n(L/2)$. (d) Amplitude of Friedel oscillations at $L/2$, δn (see text), as a function of ladder length L . The lines are linear fits. Circles, squares, and diamonds correspond to $\delta_e = 0.0833, 0.125$, and 0.25 , respectively.

fects caused by the open boundary conditions of our ladders [26, 30], we calculate $P(r)$ from an average of N_{avg} correlations of the same distance r , centered about the midpoint of the ladder. The results shown here used $N_{\text{avg}} = 10$ ($N_{\text{avg}} = 11$) for even (odd) r . In Fig. 2, we show the normalized pair-pair correlation function ($P(r)/P(r = 1)$) for 96-rung ladders with $U_d = 8$, $U_p = 3$, $t_{pp} = 0.5$, and a range of dopings. We find that $P(r)$ is well fit by a power law $P(r) \sim r^{-\alpha}$ over a range of electron and hole dopings. As can be seen in Fig. 2, there is a very clear difference in the power law exponent for hole versus electron doping, with a noticeably faster decay with distance for hole-doped ladders. For electron doping, $\alpha < 1$ over a large range of doping, corresponding to a correlation exponent $K_\rho > 1$, which indicates quasi-long-range superconducting order. In contrast, $K_\rho < 1$ for hole doping [30]. With increased hole doping, pair correlation decays *faster* with distance [30].

A more accurate approach to determining the correlation exponent K_ρ in DMRG calculations is to fit the

charge density (Friedel) oscillations caused by the open boundaries of the ladder [26, 41]. This method also permits more accurate extrapolation of K_ρ to the $L \rightarrow \infty$ limit [26]. We use the following fitting function for the charge density n_k [26, 30, 41],

$$n_k = n_0 + A \frac{\cos(N\pi k/L_{\text{eff}} + \phi)}{\sin(\pi k/L_{\text{eff}})^{K_\rho/2}}. \quad (3)$$

In Eq. 3 n_0 is the background charge density, A the Friedel oscillation amplitude, ϕ a phase shift, and L_{eff} an effective length. Typically L_{eff} is smaller than L to account for end effects [26]. The amplitude of the charge density oscillations at the center of the system, $\delta n = n(L/2) - n_0$, scales as $L^{-K_\rho/2}$. Finite-size scaling of δn , where the values of n_0 and $n(L/2)$ are determined from the fitted function in Eq. 3, then yields the most precise estimates for the correlation exponent K_ρ in the infinite-length limit ($L \rightarrow \infty$) [26].

In Figs. 3(a)-(c) we show the Friedel oscillations of local charge density n_k on a 96-rung ladder with $U_d = 8$, $U_p = 3$, and $t_{pp} = 0.5$ for three different values of electron doping ($\delta_e = 0.0833, 0.125$, and 0.25). For each doping level we also provide estimates for both n_0 and $n(L/2)$ in Figs. 3(a)-(c). As expected, the wavelength of the Friedel oscillations is reduced with increasing doping δ_e . In Fig. 3(d) we show the finite-size scaling analysis for different ladder lengths of up to $L = 96$ to determine the correlation exponent K_ρ in the $L \rightarrow \infty$ limit.

In Fig. 4 we summarize the extrapolated values of K_ρ for two sets of parameters most relevant to cuprates in both hole- and electron-doped systems. The values of K_ρ for hole doping are from Ref. 30. We find that for electron doping, $K_\rho > 1$ and K_ρ remains nearly constant over a wide doping range. In contrast, for hole doping K_ρ is close to 1 for very small δ_h , but rapidly decreases with δ_h and is significantly less than 1 for $\delta_h > 0.0625$. These results, consistent with calculations of pair-binding energies, show that a superconducting Luther-Emery phase occurs in the electron-doped cuprate ladder but not the hole doped ladder.

The most important conclusion from our work is that the doping asymmetry in pairing correlations found within the one-band model calculations for the 2D layer [17, 20, 22] occurs also within the two-leg three-band cuprate ladder Hamiltonian for realistic Hubbard and hopping parameters. As in the one-band ladder, the three-band two-leg ladder also contains rung-based spin singlets, now on Cu-O-Cu rungs, as evidenced from the large Δ_s in the undoped ladder (Fig. 1(a)). Doping with electrons therefore generates Cu^{2+} ion pairs on the rungs, and superconducting correlations persist for the same reason as in the one-band model. Doped holes create O^{1-} ions on rung or leg O-sites with equal probability. Even when a doped hole occupies a rung O-ion, a second doped hole necessarily occupies a neighboring leg oxygen, which cannot be associated with any specific rung. This severely reduces the hole-hole binding energy leading to fast decrease of the spin gap (Fig. 1(a)). Direct O-O

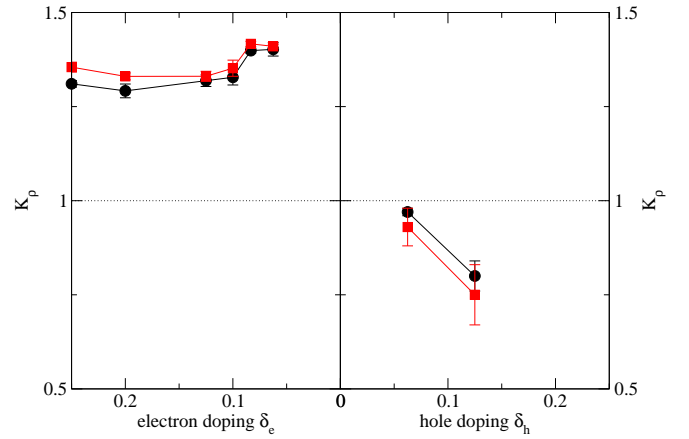


FIG. 4. (Color online) The doping dependence of the extrapolated power-law exponents K_ρ . Circles and squares are for $(U_p, t_{pp}) = (3, 0.5)$ and $(4, 0.6)$, respectively. Error bars are estimated from the fits in Fig. 3(c). Lines are guides to the eye.

hopping t_{pp} is strongly pair-breaking, as is indeed found from our calculations. This particular result has strong implications for the 2D lattice, where individual O-atoms also cannot be associated with any single Cu^{2+} -ion and each O-atom is coupled to four other oxygens. The pair-breaking effect due to O-O hopping therefore remains strong in 2D: absence of pairing in the hole-doped three-band ladder necessarily implies the same for 2D. With hindsight, this breakdown of the Zhang-Rice reduction of the full three-band Hamiltonian to a single-band Hubbard Hamiltonian is to be anticipated, as the original derivation by Zhang and Rice had excluded O-O hopping [1].

Superconductivity with electron-doping within the three-band ladder similarly predicts the same in 2D within the three-band Hamiltonian. Electron-doping generates spinless Cu^{2+} ions in the background antiferromagnet now instead of a spin-singlet ground state as O^{2-} ions remain closed-shell. O-O hopping thus plays no role whatsoever, and Cu^{2+} - Cu^{2+} pairing, as found within the one-band Hamiltonian will persist within the three-band Hamiltonian. Coexistence with long-range antiferromagnetism (AFM), as is found in the one-band calculations, is a necessary condition of such pairing. Such coexistence with long-range AFM is precluded experimentally from inelastic neutron scattering studies [42] and muon spin rotation measurements [43]. Additionally, coexistence with AFM leads to coupled $d_{x^2-y^2}$ and triplet pairing, as has indeed been found within both t - t' - J and t - t' - t'' - J and Hubbard model calculations [8, 17, 20] also in contradiction to experiments. We note that a recent extended t - J model DMRG calculation on 4- and 6-leg cylinders found dominant pairing correlations and exponentially decaying spin correlations for electron doping [18]. Because even-leg cylinders are expected to possess spin gaps, distinguishing between long-range AFM and

spin gap behavior is however difficult in DMRG calculations, and these results do not necessarily contradict those obtained in references [17, 20] or here.

Rather than asymmetry, recent experiments have revealed deep underlying symmetry between hole- and electron doped cuprates [44, 45]. In both cases there is absence of coexistence between long-range AFM and SC, and there exists a quantum critical point with Fermi surface reconstruction inside the superconducting dome, accompanied by a sudden change in the number of charge carriers. In both hole- and electron-doped compounds the carrier density is linear in doping p for small doping, but jumps to $1 + p$ and $1 - p$ respectively following the Fermi surface reconstruction. The quantum critical point in hole-doped systems occurs at the doping concentration p_c where the pseudogap vanishes at zero temperature. The region between this critical doping and the doping at which SC ends in both cases is occupied by a strange metal that exhibits resistivity linear in temperature T and magnetoresistance linear in magnetic field H [44–46]. Similar behavior has now been observed in many different families of unconventional superconductors [47–50]. Many authors have therefore speculated that there is an intimate relationship between the quantum criticality and superconductivity. Very recent research indicates that charge carriers in the strange metallic state of $\text{YBa}_2\text{Cu}_3\text{O}_7$ may be charge $2e$ bosons [51]. All the above continue to be challenging within standard models of cuprate SC.

We end this Letter by pointing out that the quantum criticality and associated phenomena can be qualitatively understood within a valence transition theory of cuprates we have recently proposed [52–54]. Within this theory the Fermi surface reconstruction in both hole and electron-doped compounds is due to dopant-induced transition from positive to negative charge transfer gap state. The transition involves change in Cu-ion ionicity

from Cu^{2+} to Cu^{1+} , resulting in transfer of nearly all Cu-ion $d_{x^2-y^2}$ holes to the O-ions. Similar quantum critical transitions between different ionicities have been widely discussed over four decades in the context of neutral-ionic transition in organic donor-acceptor charge-transfer solids [55] and heavy fermion systems [56]. Carrier densities of $1 + p$ and $1 - p$ holes are naturally expected within this approach following the valence transition. Transport in the normal and superconducting states with both hole- and electron doping then involve the nearly $\frac{3}{4}$ -filled strongly correlated O-band alone, explaining the mysterious symmetry between the two cases. Previous calculations on the single-band 2D $\frac{3}{4}$ -filled Hubbard Hamiltonian have shown that (a) precisely at this carrier concentration there is a strong tendency to transition to a paired-electron crystal (PEC), which is a charge-ordered state of spin-singlet electron pairs [57, 58], and (b) very close to this concentration there occurs enhancement of superconducting pair correlations by the Hubbard U [59, 60]. In the absence of phase coherence the spin-coupled electron pairs can conceivably be the bosonic charge carriers in the strange metallic state. Importantly, the occurrence of the strange metallic state under pressure in the organic superconductor $(\text{TMTSF})_2\text{PF}_6$ [47], known to possess a $\frac{1}{4}$ -filled hole band ($\frac{3}{4}$ -filled electron band) is indirect confirmation of this approach. These and related topics are currently under investigation.

Work at Arizona was supported by National Science Foundation (NSF) grant NSF-CHE-1764152. Some of the calculations were performed using high performance computing resources maintained by the University of Arizona Research Technologies department and supported by the University of Arizona Technology and Research Initiative Fund (TRIF), University Information Technology Services (UITS), and Research, Innovation, and Impact (RII).

-
- [1] F. C. Zhang and T. M. Rice. Effective Hamiltonian for the superconducting Cu oxides. *Phys. Rev. B*, 37:3759(R)–3761(R), 1988.
 - [2] A. I. Lichtenstein and M. I. Katsnelson. Antiferromagnetism and d-wave superconductivity in cuprates: A cluster dynamical mean-field theory. *Phys. Rev. B*, 62:R9283–R9286, 2000.
 - [3] Th. Maier, M. Jarrell, Th. Pruschke, and J. Keller. d-wave superconductivity in the Hubbard model. *Phys. Rev. Lett.*, 85:1524–1527, 2000.
 - [4] David Sénéchal, P.-L. Lavertu, M.-A. Marois, and A.-M. S. Tremblay. Competition between antiferromagnetism and superconductivity in high- T_c cuprates. *Phys. Rev. Lett.*, 94:156404, 2005.
 - [5] M. Capone and G. Kotliar. Competition between d-wave superconductivity and antiferromagnetism in the two-dimensional Hubbard model. *Phys. Rev. B*, 74:054513, 2006.
 - [6] S. S. Kancharla, B. Kyung, D. Sénéchal, M. Civelli, M. Capone, G. Kotliar, and A.-M.S. Tremblay. Anomalous superconductivity and its competition with antiferromagnetism in doped Mott insulators. *Phys. Rev. B*, 77:184516, 2008.
 - [7] E. Gull, O. Parcollet, and A. J. Millis. Superconductivity and the pseudogap in the two-dimensional Hubbard model. *Phys. Rev. Lett.*, 110:216405, 2013.
 - [8] A. Foley, S. Verret, A.-M. S. Tremblay, and D. Senechal. Coexistence of superconductivity and antiferromagnetism in the Hubbard model for cuprates. *Phys. Rev. B*, 99:184510, 2019.
 - [9] M. Kitatani, R. Arita, T. Schäfer, and K. Held. Strongly correlated superconductivity with long-range spatial fluctuations. *J. Phys. Mater.*, 5:034005, 2022.
 - [10] S. Zhang, J. Carlson, and J. E. Gubernatis. Pairing correlations in the two-dimensional Hubbard model. *Phys. Rev. Lett.*, 78:4486, 1997.
 - [11] M. Qin, C.-M. Chung, H. Shi, E. Vitali, C. Hubig, U. Schollwöck, S. R. White, and S. Zhang. Absence of

- superconductivity in the pure two-dimensional Hubbard model. *Phys. Rev. X*, 10:031016, 2020.
- [12] M.-S. Vaezi, A.-R. Negari, A. Moharramipour, and A. Vaezi. Amelioration for the sign problem: an adiabatic quantum Monte Carlo algorithm. *Phys. Rev. Lett.*, 127:217003, 2021.
- [13] M. S. Hybertsen, E. B. Stechel, M. Schluter, and D. R. Jennison. Renormalization from density-functional theory to strong-coupling models for electronic states in Cu-O materials. *Phys. Rev. B*, 41:11068, 1990.
- [14] T. F. A. Müller, V. Anisimov, T. M. Rice, I. Dasgupta, and T. Saha-Dasgupta. Electronic structure of ladder cuprates. *Phys. Rev. B*, 57:R12655–R12688, 1998.
- [15] M. Hirayama, Y. Yamaji, T. Misawa, and M. Imada. Ab initio effective Hamiltonians for cuprate superconductors. *Phys. Rev. B*, 98:134501, 2018.
- [16] M. Hirayama, T. Misawa, T. Ohgoe, Y. Yamaji, and M. Imada. Effective Hamiltonian for cuprate superconductors derived from multiscale ab initio scheme with level renormalization. *Phys. Rev. B*, 99:245155, Jun 2019.
- [17] S. Jiang, D. J. Scalapino, and S. R. White. Ground-state phase diagram of the t - t' - J model. *Proc. Natl. Acad. Sci. USA*, 118:e2109978118, 2021.
- [18] S. Gong, W. Zhu, and D. N. Sheng. Robust d -wave superconductivity in the square-lattice t - J model. *Phys. Rev. Lett.*, 127:097003, 2021.
- [19] H.-C. Jiang and S. A. Kivelson. High temperature superconductivity in a lightly doped quantum spin liquid. *Phys. Rev. Lett.*, 127:097002, 2021.
- [20] S. Jiang, D. J. Scalapino, and S. R. White. Pairing properties of the t - t' - t'' - J model. *Phys. Rev. B*, 106:174507, 2022.
- [21] H. Xu, C.-M. Chung, M. Quin, U. Schollwöck, S. R. White, and S. Zhang. Coexistence of superconductivity with partially filled stripes in the Hubbard model. preprint arXiv:2303.08376, 2023.
- [22] Y.-F. Jiang, T. P. Devereaux, and H.-C. Jiang. Ground state phase diagram and superconductivity of the doped Hubbard model on six-leg square cylinders. preprint arXiv:2303.15541, 2023.
- [23] R. M. Noack, S. R. White, and D. J. Scalapino. Correlations in a two-chain Hubbard model. *Phys. Rev. Lett.*, 73:882–885, 1994.
- [24] R. M. Noack, N. Bulut, D. J. Scalapino, and M. G. Zacher. Enhanced $d_{x^2-y^2}$ pairing correlations in the two-leg Hubbard ladder. *Phys. Rev. B*, 56:7162, 1997.
- [25] L. Balents and M. P. A. Fisher. Weak-coupling phase diagram of the two-chain Hubbard model. *Phys. Rev. B*, 53:12133–12141, 1996.
- [26] M. Dolfi, B. Bauer, S. Keller, and M. Troyer. Pair correlations in doped Hubbard ladders. *Phys. Rev. B*, 92:195139, 2015.
- [27] Y. Gannot, Y.-F. Jiang, and S. A. Kivelson. Hubbard ladders at small U revisited. *Phys. Rev. B*, 102:115136, 2020.
- [28] E. Dagotto and T. M. Rice. Surprises on the way from one- to two-dimensional quantum magnets: the ladder materials. *Science*, 271:618–623, 1996.
- [29] K. Le Hur and T. M. Rice. Superconductivity close to the Mott state: From condensed-matter systems to the superfluidity in optical lattices. *Ann. Phys.*, 324:1452–1515, 2009.
- [30] J.-P. Song, S. Mazumdar, and R. T. Clay. Absence of Luther-Emery superconducting phase in the three-band model for cuprate ladders. *Phys. Rev. B*, 104:104504, 2021.
- [31] E. Jeckelmann, D. J. Scalapino, and S. R. White. Comparison of different ladder models. *Phys. Rev. B*, 58:9492, 1998.
- [32] S. Nishimoto, E. Jeckelmann, and D. J. Scalapino. Differences between hole and electron doping of a two-leg CuO ladder. *Phys. Rev. B*, 66:245109, 2002.
- [33] Steven R. White and D. J. Scalapino. Doping asymmetry and striping in a three-orbital CuO₂ Hubbard model. *Phys. Rev. B*, 92:205112, Nov 2015.
- [34] M. Fishman, S. R. White, and E. M. Stoudenmire. The ITensor software library for tensor network calculations. *SciPost Physics Codebases*, 4, 2022.
- [35] E. M. Stoudenmire and S. R. White. Real-space parallel density matrix renormalization group. *Phys. Rev. B*, 87:155137, 2013.
- [36] E. Dagotto, J. Riera, and D. Scalapino. Superconductivity in ladders and coupled planes. *Phys. Rev. B*, 45:5744–5747, 1992.
- [37] R. M. Noack, S. R. White, and D. J. Scalapino. The ground state of the two-leg Hubbard ladder A density-matrix renormalization group study. *Physica C*, 270:281, 1996.
- [38] H. Eskes and J. H. Jefferson. Superexchange in the cuprates. *Phys. Rev. B*, 48:9788, 1993.
- [39] A. Abdelwahab, G. Polat, and E. Jeckelmann. Pair binding and enhancement of pairing correlations in asymmetric Hubbard ladders. *Phys. Rev. B*, 107:125117, 2023.
- [40] A. Luther and V. J. Emery. Backward scattering in the one-dimensional electron gas. *Phys. Rev. Lett.*, 33:589–592, 1974.
- [41] S. R. White, I. Affleck, and D. J. Scalapino. Friedel oscillations and charge density waves in chains and ladders. *Phys. Rev. B*, 65:165122, 2002.
- [42] E. M. Motoyama, G. Yu, I. M. Vishik, O. P. Vajik, P. K. Mang, and M. Greven. Spin correlations in the electron-doped high-transition-temperature superconductor Nd_{2-x}Ce_xCuO_{4±δ}. *Nature*, 445:186, 2007.
- [43] H. Saadaoui, Z. Salman, H. Luetkens, T. Prokscha, A. Suter, W. A. MacFarlane, Y. Jiang, K. Jin, R. L. Greene, E. Morenzoni, and R. F. Kiefl. The phase diagram of electron-doped La_{2-x}Ce_xCuO_{4-δ}. *Nat. Commun.*, 6:6041, 2015.
- [44] C. Proust and L. Taillefer. The remarkable underlying ground states of cuprate superconductors. *Ann. Rev. Condens. Matter Phys.*, 10:409–429, 2019.
- [45] R. L. Greene, P. R. Mandal, N. R. Poniatowski, and T. Sarkar. The strange metal state of the electron-doped cuprates. *Ann. Rev. Condens. Matter Phys.*, 11:213–229, 2020.
- [46] A. Legros, S. Bernhabib, W. Tabis, F. Laliberté, M. Dion, M. Lizaire, D. Vignolles, H. Raffy, Z. Z. Li, P. Auban-Senzier, N. Doiron-Leyraud, P. Fournier, D. Colson, L. Taillefer, and C. Proust. Universal T -linear resistivity and Planckian dissipation in overdoped cuprates. *Nature Physics*, 15:142–147, 2019.
- [47] N. Doiron-Leyraud, P. Auban-Senzier, S. R. de Cotret, C. Bourbonnais, D. Jérôme, K. Bechgaard, and L. Taillefer. Correlation between linear resistivity and T_c in the Bechgaard salts and the pnictide superconductor Ba(Fe_{1-x}Co_x)₂As₂. *Phys. Rev. B*, 80:214531, 2009.
- [48] I. M. Hayes, N. Maksimovic, G. N. Lopez, M. K. Chan, B. J. Ramshaw, R. D. McDonald, and J. G. Analytis.

- Superconductivity and quantum criticality linked by the Hall effect in a strange metal. *Nature Physics*, 17:58–62, 2021.
- [49] J. Yuan, Q. Chen, K. Jiang, Z. Feng, Z. Lin, H. Yu, G. He, J. Zhang, X. Jiang, X. Zhang, Y. Shi, Y. Zhang, M. Qin, Z. G. Cheng, N. Tamura, Y.-F. Yang, T. Xiang, J. Hu, I. Takeuchi, K. Jin, and Z. Zhao. Scaling of the strange-metal scattering in unconventional superconductors. *Nature*, 602:431–436, 2022.
- [50] P. Phillips, N. E. Hussey, and P. Abbamonte. Stranger than metals. *Science*, 377:eabh4273, 2022.
- [51] C. Yang, H. Liu, Y. Liu, J. Wang, D. Qiu, S. Wang, Y. Wang, Q. He, X. Li, P. Li, Y. Tang, J. Wang, X. C. Xie, J. M. Valles Jr., J. Xiong, and Y. Li. Signatures of a strange metal in a bosonic system. *Nature*, 605:205–210, 2022.
- [52] S. Mazumdar. Valence transition model of the pseudogap, charge order, and superconductivity in electron-doped and hole-doped copper oxides. *Phys. Rev. B*, 98:205153, 2018.
- [53] S. Mazumdar. Negative charge-transfer gap and even parity superconductivity in Sr_2RuO_4 . *Phys. Rev. Res.*, 2:023382, 2020.
- [54] J.-P. Song, S. Mazumdar, and R. T. Clay. Valence transition theory of the pressure-induced dimensionality crossover in superconducting $\text{Sr}_{14-x}\text{Ca}_x\text{Cu}_{24}\text{O}_{41}$. preprint arXiv:2207.00628, 2022.
- [55] M. Masino, N. Castagnetti, and A. Girlando. Phenomenology of the neutral-ionic valence instability in mixed stack charge-transfer crystals. *Crystals*, 7:108, 2017. and references therein.
- [56] K. Miyake and S. Watanabe. Ubiquity of unconventional phenomena associated with critical valence fluctuations in heavy fermion metals. *Phil. Mag.*, 97:3495, 2017.
- [57] H. Li, R. T. Clay, and S. Mazumdar. The paired-electron crystal in the two-dimensional frustrated quarter-filled band. *J. Phys.: Condens. Matter*, 22:272201, 2010.
- [58] S. Dayal, R. T. Clay, H. Li, and S. Mazumdar. Paired electron crystal: Order from frustration in the quarter-filled band. *Phys. Rev. B*, 83:245106, 2011.
- [59] N. Gomes, W. Wasanthi De Silva, T. Dutta, R. T. Clay, and S. Mazumdar. Coulomb enhanced superconducting pair correlations in the frustrated quarter-filled band. *Phys. Rev. B*, 93:165110, 2016.
- [60] R. T. Clay and S. Mazumdar. From charge- and spin-ordering to superconductivity in the organic charge-transfer solids. *Phys. Rep.*, 788:1, 2019.